

Introduction

1. The classical approach for plume buoyancy flux implies two big assumptions: that the swell is fully isostatically compensated by the hot ponding plume material at the base of the lithosphere; and that this plume material spreads at exactly the same speed as the overriding plate moves.
2. However, hotspot swells are largely dynamically instead of fully isostatically compensated; to some extent, swells are further compensated by sublithospheric erosion^[1]. Moreover, at least some plumes spread faster than plate motion^[2,3]. Thus, classical estimates for the buoyancy fluxes of deep-seated mantle upwellings may be strongly biased by surface-plate velocities^[4].
3. As detailed estimates of dynamic seafloor topography are now available^[5], it is time to revisit the buoyancy fluxes and, thereby, the mass and heat fluxes carried by mantle plumes.

Methods

1. We use finite element method software **ASPECT** to solve momentum, mass, energy, and composition conservation of incompressible fluid under Boussinesq approximation^[6].
2. We plan to add a free surface boundary condition at the top to accurately measure the dynamic topography.
3. We adopt **composite rheology** in our models, which is defined as:

$$\frac{1}{\eta_{comp}} = \frac{1}{\eta_{diff}} + \frac{1}{\eta_{dist}}$$

$$\eta_i = \frac{1}{2} A_i \frac{1}{n_i} d^{n_i} \dot{\epsilon}_i \frac{1-n_i}{n_i} \exp\left(\frac{E_i + pV_i^*}{n_i RT}\right)$$

where i relates to dislocation creep or diffusion creep, A_i are the prefactors.

4. We carried out a series of rheology sensitivity tests.

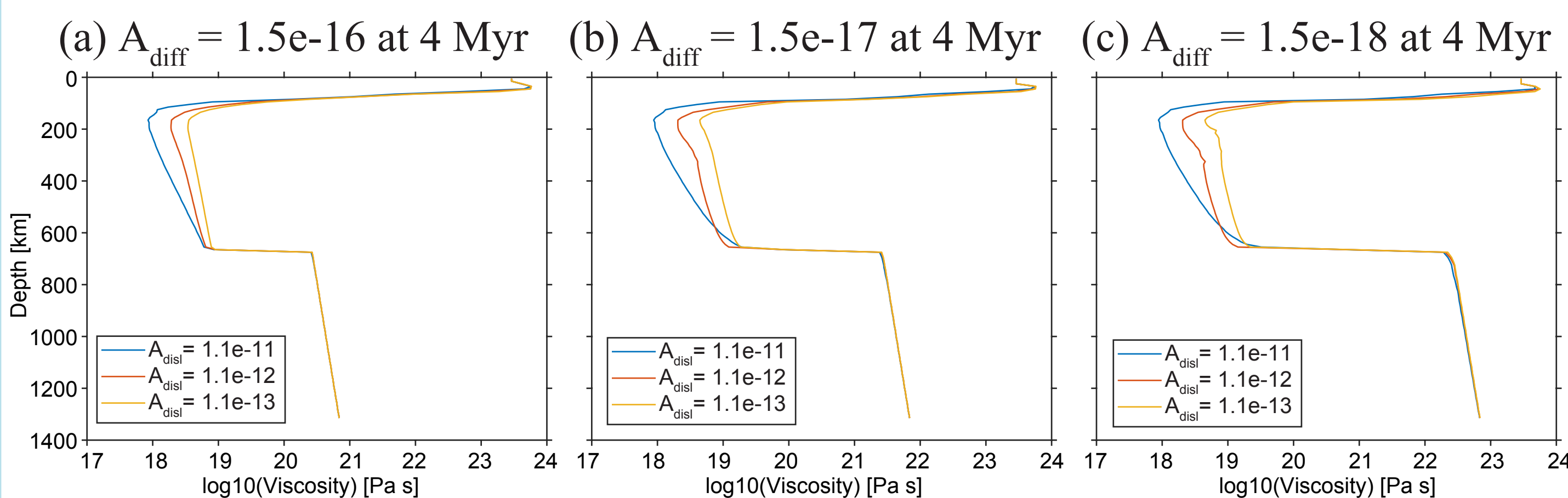


Figure 1. Viscosity profiles with various diffusion and dislocation creep prefactors

- a. When $A_{diff} = 1.5e-16$, the rheology is dominated by diffusion creep in the upper mantle, whereas $A_{diff} \geq 1.5e-17$, the upper mantle seems to be dominated by both diffusion and dislocation creep.
- b. We choose $A_{diff} = 1.5e-18$, $A_{disl} = 1.1e-13$ as our viscosity prefactors.

Preliminary results

1. Model No.1: $r_p = 68$ km, composite rheology

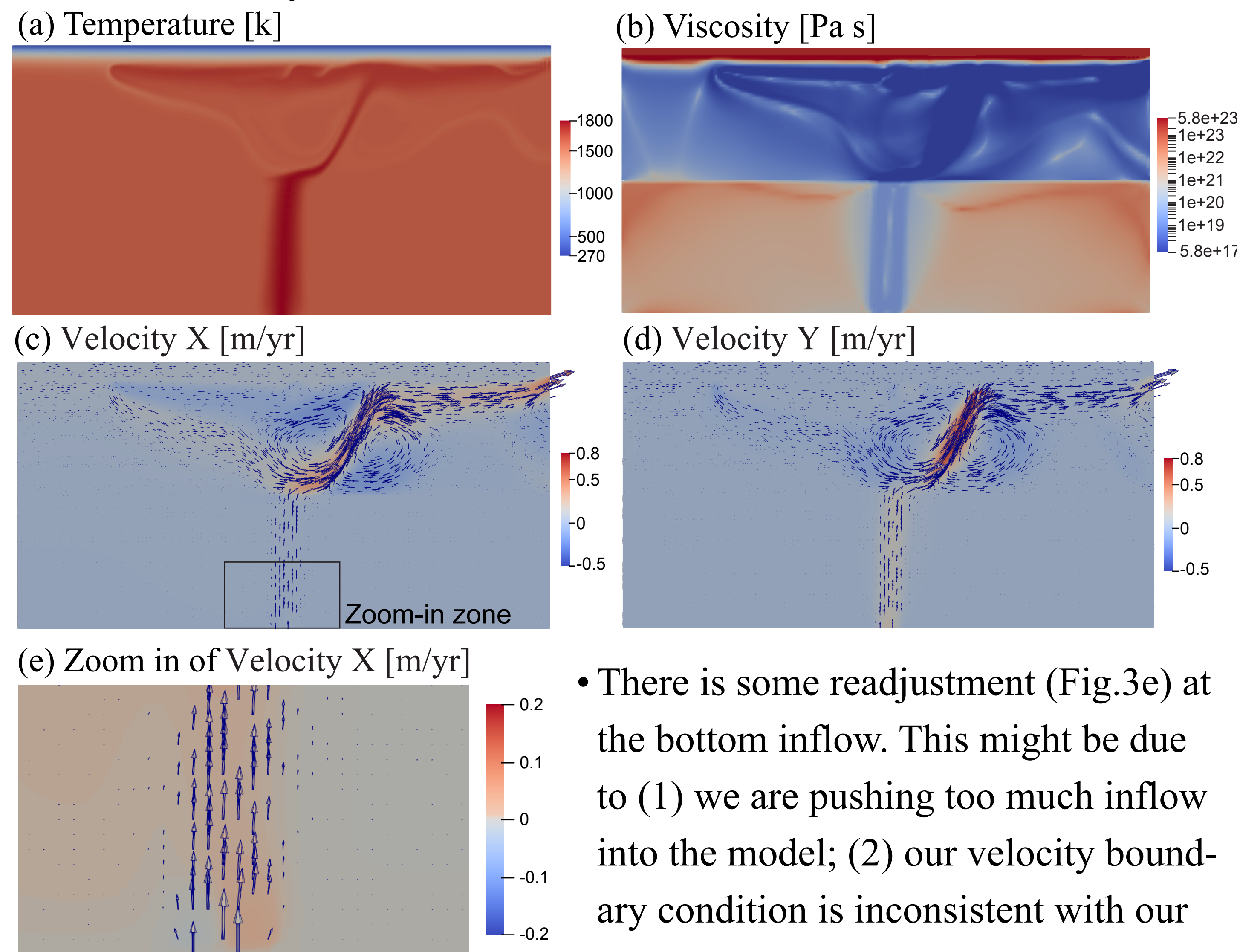


Figure 3. Model No.1 results at 20 Myr

- There is some readjustment (Fig.3e) at the bottom inflow. This might be due to (1) we are pushing too much inflow into the model; (2) our velocity boundary condition is inconsistent with our model rheology because we assume constant viscosity in calculating it.

- So we test some more cases with different bottom u_z (different plume radius, Model 2) and different rheology (constant viscosity, Model 3).

Model design

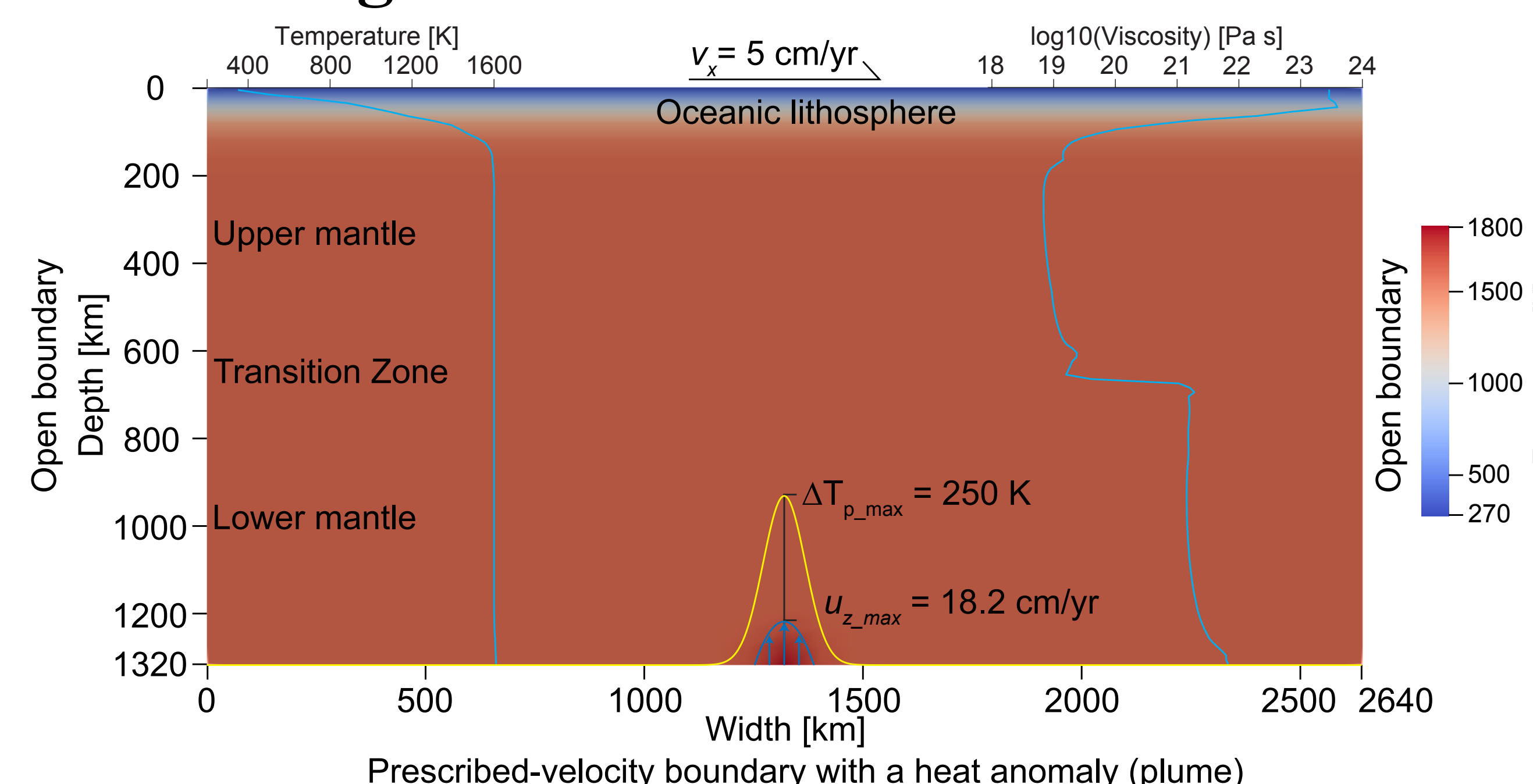


Figure 2. Temperature of the initial model setup

1. Bottom **velocity** boundary condition:

$$u_{z_bot} = \frac{1}{2\eta_0} \alpha \rho_m g \Delta T_p (r_p^2 - (x - x_0)^2)$$

2. Bottom **temperature** boundary condition:

$$T_{bot} = T_m + \Delta T_{plume} \times \exp\left(-\frac{(x - x_0)^2}{r_{plume}^2}\right)$$

2. Model No.2: $r_p = 50$ km, composite rheology

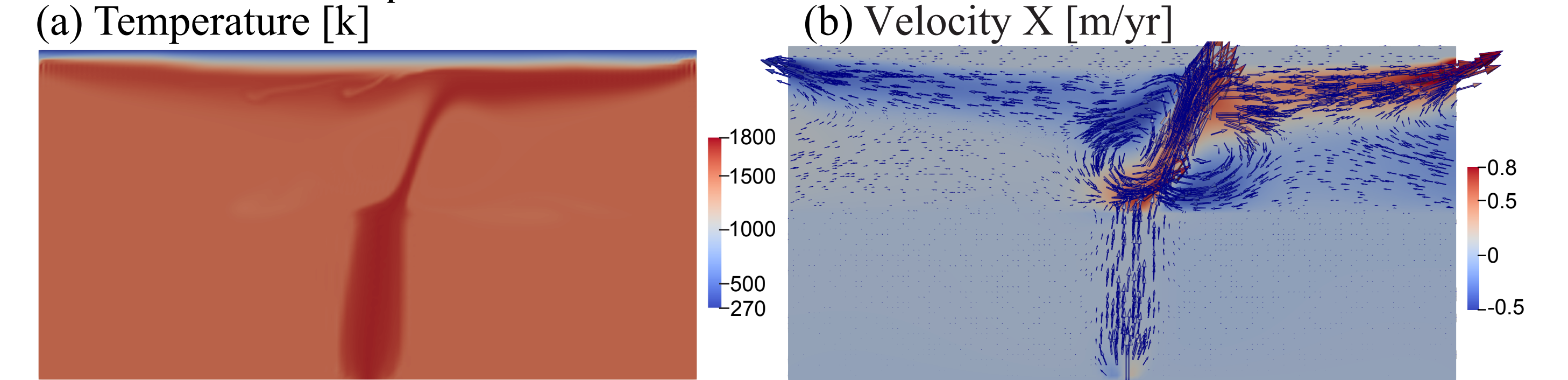


Figure 4. Model No.2 results at 20 Myr

- With bigger inflow, the radius of the plume conduit increases as it goes up, and the readjustment shown in Fig. 4b is more obvious than model 1.

3. Model No.3: $r_p = 100$ km, constant rheology

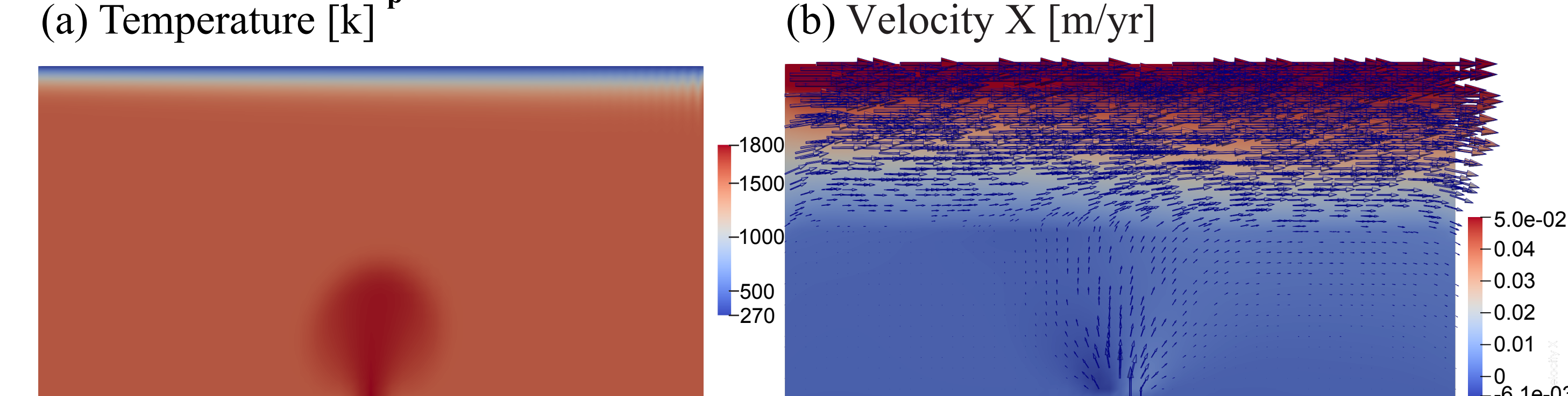


Figure 5. Model No.3 results at 50 Myr

- With constant viscosity, which is consistent with the velocity boundary conditions, there is less readjustment than model 2. So it is important to make sure that the velocity and temperature boundary conditions and the model rheology are consistent.

4. Estimate the 2D flux of different u_z of the bottom inflow

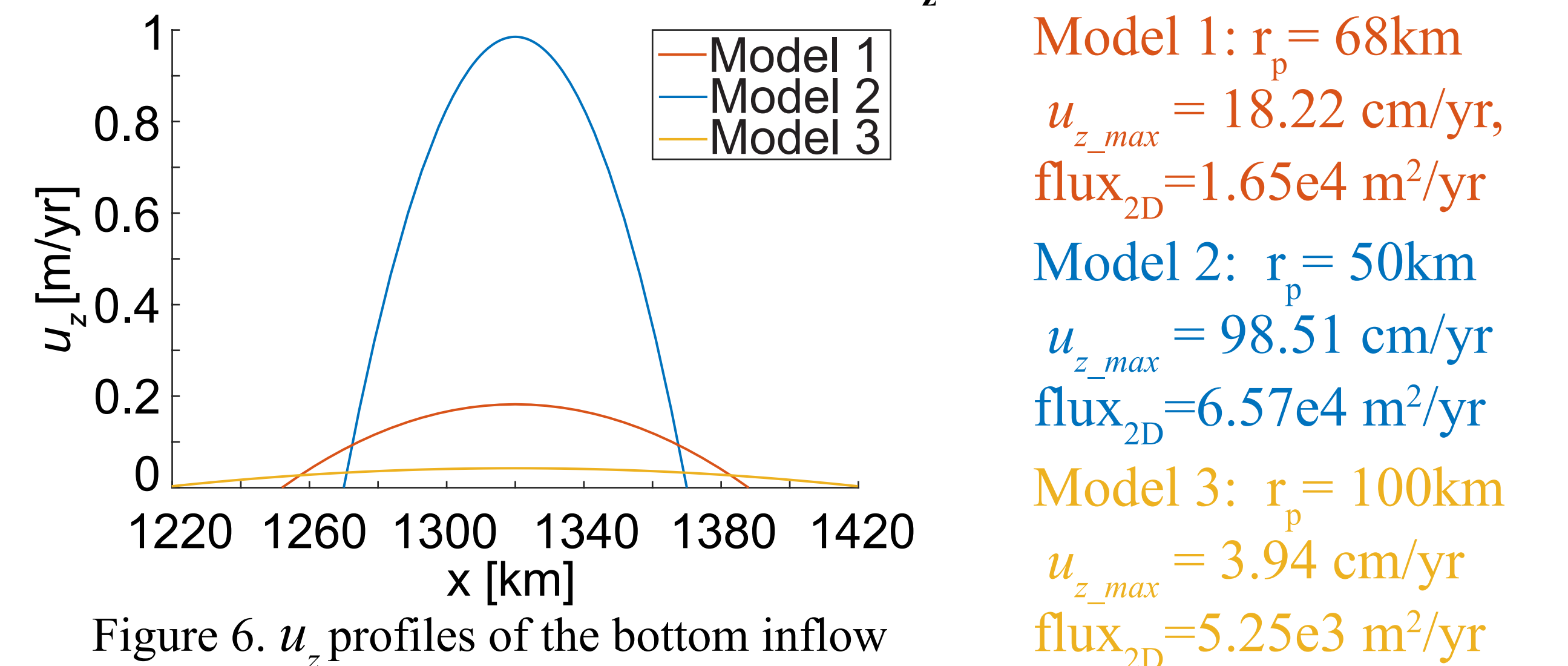


Figure 6. u_z profiles of the bottom inflow

Next steps

1. Solve the inconsistency in the bottom velocity boundary conditions and the model rheology and temperature boundary conditions.
2. Add a free surface with a moving plate at the top of the model.
3. Run 3D models.
4. To calculate the dynamic topography and compare to observations.

References

1. Cadio et al., 2012; doi:1016/j.epsl.2012.10.006
2. Ribe & Christensen, 1999; doi:10.1016/S0012-821X(99)00179-X
3. Poore et al., 2011; doi: 10.1038/ngeo1161
4. Hoggard et al., 2020; doi: 10.1016/j.epsl.2020.116317
5. Hoggard et al., 2016; doi: 10.1038/ngeo2709
6. Bangerth, et al., (2020b). ASPECT User Manual. doi:10.6084/m9.figshare.4865333